The Active Site Loop of *S*-Adenosylmethionine Synthetase Modulates Catalytic Efficiency†

John C. Taylor,‡ Fusao Takusagawa,§ and George D. Markham*,‡

Institute for Cancer Research, Fox Chase Cancer Center, 7701 Burholme Avenue, Philadelphia, Pennsylvania 19111, and Department of Molecular Biosciences, University of Kansas, Lawrence, Kansas 66045

Received March 22, 2002; Revised Manuscript Received May 22, 2002

ABSTRACT: Crystallographic studies of *Escherichia coli S*-adenosylmethionine synthetase (ATP:L-methionine *S*-adenosyltransferase, MAT) have defined a flexible polypeptide loop that can gate access to the active site without contacting the substrates. The influence of the length and sequence of this active site loop on catalytic efficiency has been characterized in a mutant in which the *E. coli* MAT sequence (DRADPLEQ) has been replaced with the distinct sequence of the corresponding region of the otherwise highly homologous rat liver enzyme (HDLRNEEDV). Four additional mutants in which the entire DRADPLEQ sequence was replaced by five, six, seven, or eight glycines have been studied to unveil the effects of loop length and the influence of side chains. In all of the mutants, the maximal rate of *S*-adenosylmethionine formation (k_{cat}) is diminished by more than 200-fold whereas the rate of hydrolysis of the tripolyphosphate intermediate is decreased by less than 3-fold. Thus, the function of the loop is localized to the first step in the overall reaction. The K_m for methionine increases in all of the oligoglycine mutants, whereas the K_m values for ATP are not substantially different. The k_{cat} for the wild-type enzyme is decreased by increases in solution microviscosity with 55% of the maximal dependence. Thus, a diffusional event is coupled to the chemical step of AdoMet formation, which is known to be rate-limiting. The results indicate that a conformational change, possibly loop closure, is associated with AdoMet synthesis. The data integrate a previously discovered conformational change associated with PPP_i binding to the E·AdoMet complex into the reaction sequence, reflecting a difference in protein conformation in the E·AdoMet·PPP_i complex whether it is formed from the E·ATP·methionine complex or from binding of exogenous PPP_i. The temperature dependence of the k_{cat} for *S*-adenosylmethionine formation shows that the removal of the side chains in the glycine mutants causes the activation enthalpy of the reaction to approximately double in each case, while the activation entropy changes from negative in the wild-type enzyme to positive in the mutants. The favorable activation entropy in the mutant-catalyzed reactions may reflect release of water during catalysis, while the negative activation entropy in the reaction catalyzed by the wild-type enzyme apparently reflects reorganization of the loop. The observations point to how nature can fine-tune the activity of an enzyme by modifying substrate and product access to the active site rather than by altering the enzyme·substrate contacts or the catalytic machinery itself.

The movement of protein segments in enzymatic catalysis is a widespread phenomenon, often related to sequestration of reactive intermediates from escape into solution and the recruitment of groups from differing segments of a polypeptide chain into a functional catalytic arrangement (*1*−*29*). Movements may be either of large polypeptide segments, such as in domain reorientation, or less grandiose as in active site lids (*9*). Rearrangements of loops that constitute active site lids may be rigid body reorientations around flexible hinges or local changes in the conformation of the polypeptide chain (*9*). In some cases, the rate of motion appears to be independent of protein ligation state while in other instances the rates are modulated by the binding of ligands (*10*, *11*, *16*, *18*, *21*, *24*−*29*). The rates of these rearrangements vary widely and have been reported on as short as the nanosecond time scale (*4*, *11*, *14*, *21*, *25*). The sequence requirements for proper function of these segments, in either the "hinges" or the central region, are as yet not well-defined, although mutagenesis studies have begun to provide insight into hinge constitution in some cases (cf. *4*, *6*, *7*, *11*, *20*, *22*, *23*, *28*).

Crystallographic studies of *S*-adenosylmethionine (AdoMet)[1] synthetase (ATP:L-methionine *S*-adenosyltransferase, methionine adenosyltransferase, MAT) have defined a polypeptide loop that has alternate conformations in different

† This work was supported by National Institutes of Health Grants GM31186 (to G.D.M.), GM37233 (to F.T.), and CA06927 (to the Fox Chase Cancer Center), and also supported by an appropriation from the Commonwealth of Pennsylvania.

* To whom correspondence should be addressed at the Institute for Cancer Research, Fox Chase Cancer Center, 7701 Burholme Ave., Philadelphia, PA 19111. Telephone: 215-728-2439; Fax: 215-728-3574; Email: GD_Markham@fccc.edu.

‡ Fox Chase Cancer Center.

§ University of Kansas.

[1] Abbreviations: AdoMet, *S*-adenosyl-L-methionine; PPP_i, tripolyphosphate; MAT, *S*-adenosylmethionine synthetase; EcMAT, wild-type *E. coli* MAT; G#-EcMAT, *E. coli* MAT with #-glycines in place of residues ^{108}DRADPLEQ; RLL-EcMAT, *E. coli* MAT with the sequence of the rat liver isozyme (HLDRNEEDV) in place of the natural ^{108}DRADPLEQ; Rl-MAT, rat liver MAT.

10.1021/bi025851t CCC: $22.00
Published on Web 06/29/2002

structures and is in a position to gate access to the active site (*30*−*32*). The functional consequences of the constitution of this loop are the subject of the present investigations. The AdoMet synthetic reaction is composed of two sequential steps, AdoMet formation and the subsequent hydrolysis of tripolyphosphate (PPP_i), which occurs prior to release of AdoMet from the enzyme, as depicted below (*33*, *34*).

$$\text{L-methionine} + \text{ATP} + H_2O \rightarrow$$
$$[\text{AdoMet} + PPP_i] + H_2O \rightarrow \text{AdoMet} + PP_i + P_i$$

Our studies of the structural and mechanistic properties of MAT are in the context of the *Escherichia coli* enzyme (herein designated EcMAT), which is a tetramer of identical 383 residue subunits with 1 active equivalent site per subunit (*35*). The crystal structure of EcMAT has been determined as the ligand-free enzyme, and in the presence of the bound products PP_i and P_i, as well as with ADP and P_i (which arose from enzymatic ATP hydrolysis in the crystals) (*30*−*32*). The more recently described structure of the highly homologous rat liver isozyme (Rl-MAT; 60% sequence identity to the *E. coli* enzyme) showed a similar protein topology, with RMS deviation among α-carbons of ca. 1.2 Å, which was considered insignificantly different than the difference between the two crystallographically independent subunits in the *E. coli* apoenzyme structure (*36*). However, the position of the methionine analogue inhibitor L-2-amino-*cis*-3,4-butenoic acid (cis-AMB) present in the Rl-MAT structure was displaced significantly from the nucleotide binding site of EcMAT. There is ca. 11 Å between the C5′ of the nucleotide at which the AdoMet-forming reaction occurs and the position in cis-AMB where the sulfur of the methionine would be located. This observation suggests that conformational rearrangements must accompany catalysis, which is in accord with pre-steady-state kinetic results with EcMAT (*37*). A structure of MAT with all of the substrate (product) binding sites occupied that would address this question has not been reported.

The active sites of both the *E. coli* and rat liver MAT reside between two subunits, with contributions from side chains of residues from both subunits, resulting in a dimer as the minimal catalytic entity. The side chains that contribute to the ligand binding sites are conserved between the two proteins. In the structures of complexes with the *E. coli* enzyme, the phosphate groups have the same positions in the (PP_i plus P_i) complex and the (ADP plus P_i) complex, and are located at the bottom of a deep cavity with the adenosyl group nearer the entrance (*31*). The only main chain conformational differences between the ligand-free and complexed enzyme structures are in a surface loop consisting of residues 100−115 (EcMAT numbering), of which residues 102−107 are disordered in all of the structures with bound ligands. However, the structure of the ligand-free enzyme revealed the surface loop in two conformations, both of which blocked the active site entrance (Figure 1) (*30*). This further indicates that conformational alterations must occur during the catalytic cycle to allow access and departure of ligands. A corresponding segment of Rl-MAT (rat liver sequence numbers 118−128) was disordered in the crystal structure (*36*). The presence of a dynamic loop gating active substrate accessibility to the active site might contribute to the slow substrate binding rates of 10^5 M^{-1} s^{-1} (*37*).

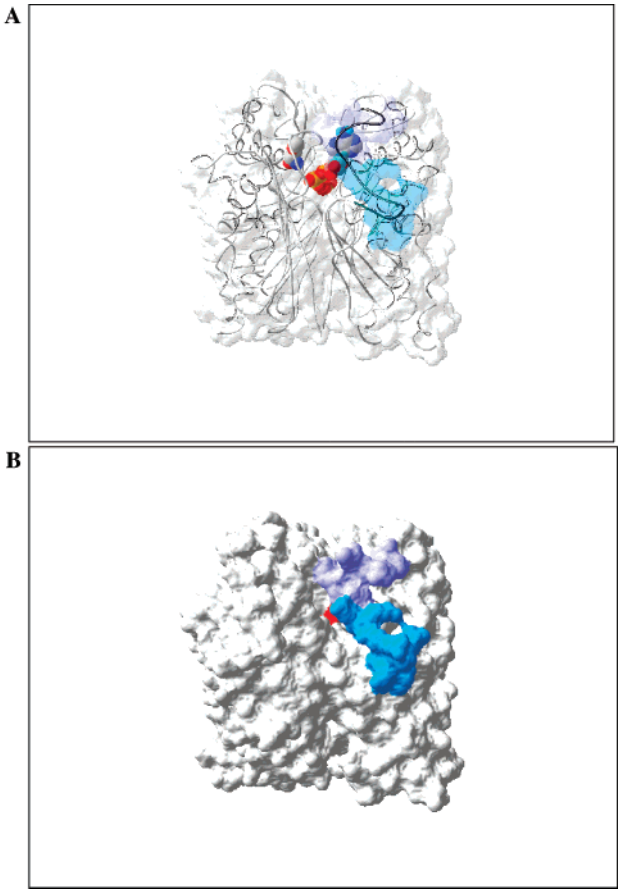

FIGURE 1: Illustrations of the flexible loop over the MAT active site. The protein surface is shown along with ADP, P_i, and the methionine analogue cis-AMB. One active site, located between two subunits of a dimer, is shown. The second active site is located at the bottom rear of the protein in the orientation of this illustration. In part A, the protein surface is transparent with the loop in blue, revealing the buried ligands and the Cα trace of the two subunits of the enzyme. In part B, the protein surface is shown as solid, and only oxygens of P_i are visible. The figure was constructed by superposition of the protein main chain of PDB files 1fug (subunit A), 1mxb, and 1qm4. The coordinates of the protein main chain in the ligand-free enzyme (PDB file 1fug, subunits A and B) and the ligand positions for ADP and P_i (from PDB file 1mxb), and the methionine analogue cis-AMB (from PDB file 1qm4) were retained.

Furthermore, kinetic analyses revealed two conformational changes which occurred when all of the ligand binding sites were occupied (*37*). Movements of a loop to gate access to the active site may relate to the competing need for substrate and product access and the sequestration therein of the PPP_i reaction intermediate.

This active site loop contains the least conserved internal region of sequence among otherwise highly homologous MATs from eucarya and bacteria. In these MATs, the variable part of the loop sequence ranges in length from 6 to 19 residues (in *Bacillus subtilis* and *Thermotoga maritima*, respectively), with lengths of 7−11 residues being the most common in the sequence databases. The boundaries of the loop are clear, being well-defined and consistently positioned in the crystal structures, and highly conserved in sequence. The variability of the MAT loop sequence contrasts with the highly conserved sequences of active site loops in many enzymes, and makes elucidation of the functional roles particularly challenging. The present study has investigated the contributions of diffusional steps to the catalytic rates

and the influence of the length and sequence of this active site loop on enzyme function. The results confirm that the constitution of this loop dramatically and selectively influences the efficiency of the enzyme in catalyzing AdoMet formation.

EXPERIMENTAL PROCEDURES

Reagents were purchased from Sigma unless noted. AdoMet was obtained from Research Biochemicals International. L-[*methyl*-^{14}C]Methionine was purchased from DuPont-NEN. Ecoscint scintillation fluid was from National Diagnostics. The *E. coli* strains used were XL1-Blue and RSR15(DE3). RSR15(DE3) is a *metK* derivative of strain BL21(DE3); extracts of this strain have no detectable MAT activity (*38*).

Oligonucleotides used in mutagenesis were prepared in the Fannie Ripple Biotechnology Facility at the Fox Chase Cancer Center. The altered DNA sequence of the rat liver loop mutant (RLL-EcMAT) was verified as CACCTTGATCGCAATGAGGAGGATGTG in place of the wild-type sequence GACCGTGCCGATCCGCTGGAACAG. This mutant was constructed using the uracil enrichment method (*39*) with plasmid pTZK which has the *E. coli metK* gene inserted between the *Pst*I and *Eco*RI sites of plasmid pTZ18U (*40*). The oligoglycine mutants were subsequently constructed using the Quikchange kit (Strategene). The wild-type EcMAT sequence in plasmid pT7K was used to construct the glycine-5 mutant because this pT7-6 derivative routinely yields higher levels of protein expression than pTZK (*38*). The glycine-5 mutant was then used as template for construction of the glycine-6, -7, and -8 variants. The variable regions of the G#-EcMAT mutants contained five to eight repeated GGC triplets in place of the wild-type sequence. Preliminary studies of RLL-EcMAT were described previously (*41*).

Plasmid DNA was purified from ampicillin-resistant transformants using the Wizard Plus Miniprep DNA Purification System (Promega Corp., Madison, WI). Mutants were identified by automated DNA sequencing in the Fox Chase core facility. Complete DNA sequences confirmed that only the designated mutations were present.

Enzyme Purification and Characterization. Plasmids were transformed into strain RSR15(DE3) for protein isolation. Cultures were grown in LB media containing 50 μg/mL carbenecillin. Following overnight growth, protein expression was enhanced by addition of 0.1 mM isopropyl-1-thio-(β-D-galactopyranoside for 30 min prior to harvesting. Wild-type and mutant MATs were purified by ammonium sulfate fractionation followed by successive chromatography on hydrophobic interaction matrix Phenyl-Sepharose HR (Pharmacia) and Hydroxylapetite CHT-I (BioRad), and by anion exchange on Aminohexyl-Sepharose (EAH-4B, Pharmacia) (*38*). The enzymes were electrophoretically homogeneous.

MATs were analyzed for oligomerization state by native gel electrophoresis of 20 μM enzyme samples on 8−25% gradient gels (*38*). Native molecular masses were also compared by gel filtration on Superdex-200 in 50 mM Tris·HCl, 100 mM KCl, 40 mM $MgCl_2$, 0.1 mM DTT buffer; the protein concentration was 3 μM, comparable to the concentration used for the mutants in the kinetic studies of the overall reaction (10 μM).

Secondary structures were assessed from circular dichroism (CD) spectra recorded on an Aviv model 62A spectropolarimeter. Samples (7 μM protein in 25 mM Tris·HCl, 25 mM KCl, pH 8.0) were placed in 1 mm path length cells; spectra were recorded from 200 to 260 nm and were corrected for buffer contributions

Enzyme Activity Assays. MAT activity was determined by the [^{14}C]AdoMet cation-exchange filter binding method (*40*). Assays were performed in the presence of various concentrations of ATP and L-[*methyl*-^{14}C]methionine in 50 mM Hepes·$(CH_3)_4N^+$ at pH 8.0 with 50 mM KCl, and 50 mM $MgCl_2$. The tripolyphosphatase activity was determined by quantifying orthophosphate production (*42*). Assays contained 50 mM Hepes·$(CH_3)_4N^+$ at pH 7.8 with 10 mM KCl and 10 mM $MgCl_2$.

Substrate saturation data were evaluated using standard kinetic equations as implemented in the kinetics module of Sigmaplot 2000 (SPSS Software) or the program Enzfitter (Elsevier Biosoft). For the overall reaction, data were fit to the equation:

$$V = V_{max}[\mathrm{ATP}][\mathrm{methionine}]/(K_{\mathrm{ATP}}K_{\mathrm{m,methionine}} + K_{\mathrm{m,methionine}}[\mathrm{ATP}] + K_{\mathrm{m,ATP}}[\mathrm{methionine}] + [\mathrm{ATP}][\mathrm{methionine}])$$

where $V_{max} = k_{cat}{\cdot}E$, K_m values are the Michaelis constants at saturating cosubstrate concentrations, and K values are the Michaelis constants extrapolated to zero cosubstrate concentration (*43*, *44*). Data for PPP_i hydrolysis were fit to the one-substrate Michaelis−Menten equation. Uncertainties in kinetic constants are listed in the tables.

Viscosity Dependence of Kinetic Parameters. Solution microviscosities were modified by addition of sucrose. Viscosities, η, were determined at 25 °C using an Ostwald viscometer (*45*). Viscosities are reported relative to that measured for a solution of reaction buffer lacking viscogen, η^0. Relative viscosities for solutions containing 10%, 20%, and 30% sucrose were 1.25, 1.74, and 2.70, respectively. Control experiments with solutions containing Ficoll (a ~400 000 kDa polymer) at a relative viscosity of 2.5 showed no influence of macroviscosity on either k_{cat} or k_{cat}/K_m.

Data were analyzed as the effect of relative viscosity, η/η^0, on relative $k_{cat} = (k_{cat}^0/k_{cat})$ and relative $k_{cat}/K_m = (k_{cat}/K_m)^0/(k_{cat}/K_m)$ values, where k_{cat}^0 and $(k_{cat}/K_m)^0$ are the values in the absence of viscogen where the viscosity is η^0. Data for k_{cat}/K_m were extrapolated to saturating concentrations of cosubstrate so that the k_{cat}/K_m values reflect formation of the ternary E·ATP·methionine from a binary complex (*45*). In this case, the concentration dependence of the rate of product formation measures the steps:

$$\mathrm{E{\cdot}ATP} + \mathrm{methionine} \underset{k_{-3}}{\overset{k_3}{\rightleftharpoons}} \mathrm{E{\cdot}ATP{\cdot}methionine} \underset{k_{-5}}{\overset{k_5}{\rightleftharpoons}} \mathrm{E{\cdot}AdoMet{\cdot}PPP_i} \leftrightharpoons \mathrm{products}$$

or

$$\mathrm{E{\cdot}methionine} + \mathrm{ATP} \underset{k_{-4}}{\overset{k_4}{\rightleftharpoons}} \mathrm{E{\cdot}ATP{\cdot}methionine} \underset{k_{-5}}{\overset{k_5}{\rightleftharpoons}} \mathrm{E{\cdot}AdoMet{\cdot}PPP_i} \leftrightharpoons \mathrm{products}$$

The complete kinetic scheme for the reaction is illustrated

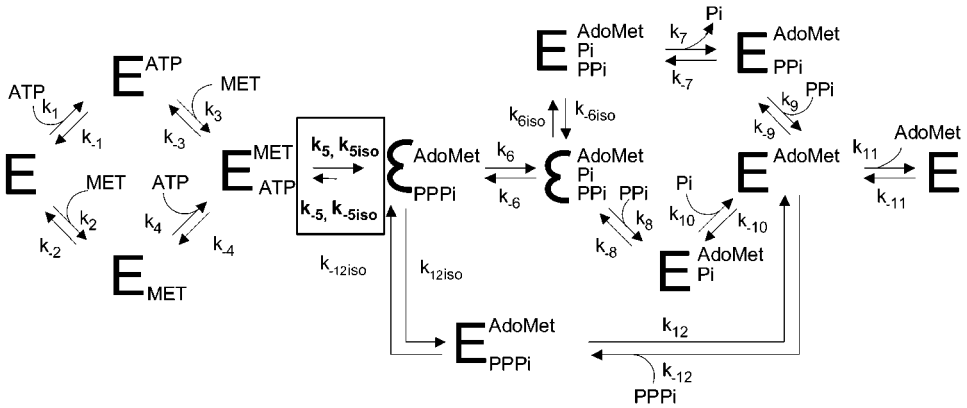

FIGURE 2: Kinetic scheme for MAT. Isomerized forms of complexes are indicated by the change in font for the enzyme from E to $\mathcal{E}$. The viscosity-dependent step influencing k_{cat} is included in $k_{\pm5}$ and is noted in the text as $k_{\pm5,iso}$ in keeping with designations for other isomerization steps. Values of kinetic constants have been previously determined for the wild-type enzyme as: $k_{+1} = 8.6 \times 10^3$ M^{-1} s^{-1}, $k_{-1} = 8$ s^{-1}; $k_{+2} = 2.5 \times 10^5$ M^{-1} s^{-1}, $k_{-2} = 150$ s^{-1}; $k_{+3} = 1.6 \times 10^5$ M^{-1} s^{-1}, $k_{-3} = 15$ s^{-1}; $k_{+4} = 1.6 \times 10^4$ M^{-1-}s^{-1}, $k_{-4} = 5$ s^{-1}; $k_{+5} = 1.5$ s^{-1}, $k_{-5} = 0.00015$ s^{-1}; $k_{+6} = 9$ s^{-1}, $k_{-6} = 14$ s^{-1}; $k_{+6,iso} = 12$ s^{-1}, $k_{-6,iso} = 0.04$ s^{-1} ; $k_{+7} = 310$ s^{-1}, $k_{-7} = 4.5 \times 10^4$ M^{-1} s^{-1}; k_{+8} = not determined; $k_{+9} = 4$ s^{-1}, $k_{-9} = 6.5 \times 10^4$ M^{-1} s^{-1}; k_{+10}, not determined; $k_{+11} = 3.4$ s^{-1}, $k_{-11} = 2.5 \times 10^5$ M^{-1} s^{-1}; $k_{+12} = 1.1 \times 10^5$ M^{-1} s^{-1}, $k_{-12} = 0.44$ s^{-1}; $k_{+12,iso} = 33$ s^{-1}, $k_{-12,iso} = 4$ s^{-1} (*37*). Steps in the route including K_8 and K_{10} are not on the major kinetic pathway (*37*). Lower limits on $k_{\pm5,iso}$ are $k_{+5,iso} = 22$ s^{-1} and $k_{-5,iso} = 14$ s^{-1}.

in Figure 2 (*37*). Since k_{-5} is ~10^{-4} of k_5, and k_6, as well as all other forward rate constants, the mechanism effectively becomes irreversible at the AdoMet formation step.

Following Adams and co-workers (*45*), the slope of a plot of (k_{cat}^0/k_{cat}) vs (η/η^0) is

$$k_{cat}^{\eta} = k_5/(k_5 + k_{fwd})$$

where k_{fwd} is the net rate constant for steps after AdoMet formation. A similar relationship holds for k_{cat}/K_m, where a plot of $(k_{cat}/K_m)^0/(k_{cat}/K_m)$ vs (η/η^0) yields

$$(k_{cat}/K_m)^{\eta} = k_5/(k_5 + k_{off})$$

where k_{off} is the dissociation rate constant for the substrate from the ternary E·ATP·methionine complex. In the cases of methionine or ATP as varied substrate, $k_{off} = k_{-3}$ and k_{-4}, respectively. Since $k_{\pm5}$ represent the rate-determining chemical reaction of AdoMet formation, these rate constants would not be sensitive to viscosity in the absence of a concomitant protein structural change. Since k_{cat}/K_m includes the substrate dissociation step, there can be a viscosity dependence if the substrate dissociation rate is slower than or comparable to the rate of catalysis. Using the previously published rate constants listed in the legend to Figure 2, estimates for $(k_{cat}/K_m)^{\eta}$ are ~0.09 for methionine and ~0.25 for the more slowly dissociating ATP.

Thermodynamics of AdoMet Synthesis. To evaluate the effects of loop sequence alteration on the thermodynamic parameters for catalysis, k_{cat} and K_m values were determined in the temperature range 0−37 °C; care was taken to ensure that initial rates were measured. The solution pH did not vary by more than 0.1 pH unit over this temperature range; the k_{cat} for the enzyme does not vary significantly over more than 2 pH units at 25 °C (*35*, *46*). The activation energy, E_a, was calculated from an Arrhenius plot of ln(k_{cat}) vs $1/T$ (slope = $-E_a/R$). The free energy of activation, $\Delta G^{\#}$, was calculated as $\Delta G^{\#}_{310} = RT\,[\ln(k_B T/h) - \ln(k_{cat})]$ where $R = 1.9872$ cal/(mol·K), k_B is the Boltzmann constant, and h is Planck's constant. The activation enthalpy, $\Delta H^{\#}_{310}$, was calculated as ($E_a - RT$). The activation entropy, $\Delta S^{\#}_{310}$, was then obtained as $(\Delta H^{\#}_{310} - \Delta G^{\#}_{310})/T$.

Molecular Modeling of Loop Mutations. To visualize potential conformations of the active site loop and the effects of mutations, models were constructed based on the available crystal structures of EcMAT. The crystallographic coordinates of the ligand-free enzyme, in which the loop is visible in both subunits of the asymmetric dimer, were utilized (PDB file 1fug, 3.2 Å resolution). Initially the protein structure was adapted to the AMBER force field (*47*) as implemented in the program MacroModel [(*48*, *49*); v. 7.0, Schrodinger Inc., 2000]. Hydrogens were added to the polar heteroatoms as appropriate; CH groups were treated as united atoms. The entire protein dimer (7254 atoms) was then subjected to 500 cycles of a constrained conjugate gradient energy minimization in which the crystallographically defined atoms were allowed to deviate by 0.1 Å from their observed positions without energy penalty, beyond which a restraining force of 120 kcal/Å was applied. The GB/SA continuum aqueous solvation model was used in all calculations to reduce the tendency for formation of adventitious polar intramolecular interactions without the computational expense of including explicit water molecules (*50*). Cutoffs of 8 and 20 Å were used for nonbonded and electrostatic interactions, respectively. The non-hydrogen atoms in the minimized structure had an overall RMS deviation of 0.1 Å from the initial structure, and the energy gradient was reduced to 0.01 kcal/(Å·mol). This structure was used as input to further modeling.

To obtain physically reasonable models of alternate loop conformations, a Monte Carlo conformational search was performed for residues 98−116 of both loops. All other residues containing atoms within 20 Å of any loop atom were included as frozen shell; i.e., their steric and electrostatic effects were included but their atomic positions were fixed. This truncation appears to be a reasonable approximation since the backbone and side chain conformations of these residues are essentially superimposable in the six available independent crystal structures of EcMAT. Five hundred steps of a low-mode Monte Carlo search were performed (*51*, *52*). The simulation included 342 mobile atoms and a fixed shell

Table 1: Loop Region Sequences of EcMAT and Mutants

designation	protein sequence
MAT (wild type)[a]	[101]dinqgvDRADPLEQ**gagdq**
RLL-MAT[b]	HLDRNEEDV
G8-MAT	GGGGGGGG
G7-MAT	GGGGGGG
G6-MAT	GGGGGG
G5-MAT	GGGGG

[a] Five amino acid residues are shown in lower case on either side of the altered region (underlined). Residues in boldface are the MAT "signature sequence." Residues 102−107 (INQGVD) were not visible in the crystal structures of six enzyme•ligand complexes (*30*−*32*). [b] In the crystal structure of the rat liver enzyme, residues 117−128 (*DIAQCV*HLDRNEE) were not visible (*36*); the underlined residues are part of the region previously defined as the flexible loop, and the italicized residues correspond to the *E. coli* sequence starting at residue 101. The **GAGDQ** signature sequence for AdoMet synthetases begins at residue 131 in the rat liver sequence.

of 1440 atoms. The mobile atoms were allowed to move by 3−6 Å in each Monte Carlo step, and then the structure was minimized. Structures with energies within 12 kcal/mol of the minimum were visually examined. A similar approach has been used to obtain useful models of the crystallographically undefined loops of the enzyme luciferase (*53*−*55*).

In the simulation, the steric energy of the lowest energy wild-type loop conformer decreased by 145 kcal/mol from the energy of the lowest energy original crystallographic conformation (chain A; chain B was 17 kcal/mol higher in steric energy). The solvation energy was 46 kcal/mol less in the modeled conformer. In an alternate approach, the positions of residues 102−107 were built randomly in an extended conformation onto subunit A from PDB file 1mxb in which these residues are not resolved, and the search was conducted as above. Conformations were obtained with larger solvent-accessible surface areas but indistinguishable steric energies from those found in the first approach.

A model for the glycine-8 mutant was constructed by removing the side chains from the DRADPLEQ sequence in one subunit (PDB file 1fug, chain A) of the minimized protein, followed by a Monte Carlo simulation of 500 steps as described above for the wild-type protein. A model of the glycine-5 mutant was constructed by deletion of three central glycines from loop, joining the fragmented chain, followed by energy minimization and Monte Carlo simulation.

RESULTS

The functional significances of the variable region of the active site loop of MAT were explored using mutants of the *E. coli* MAT (EcMAT). Mutants were designed based on the sequence of the well-characterized rat liver MAT (Rl-MAT), as well as with various lengths of oligo-glycine to remove side chain contributions and to allow length variation without additional sequence bias or introduction of a tendency toward a particular type of secondary structure (see Table 1). Each mutant was purified to homogeneity in the same manner as the wild-type enzyme. All variants were tetrameric, as judged by both gel filtration and native gel electrophoresis, and were indistinguishable by CD spectroscopy, indicating maintenance of common quaternary and secondary structures. Thus, the functional influences of the mutations apparently reflect localized alterations.

Table 2: Kinetic Parameters for AdoMet Synthesis[a]

enzyme	k_{cat}[b] (s^{-1})	K_m, ATP (mM)	K_m, Met (mM)	K, ATP (mM)	K, Met (mM)
wild-type EcMAT	1.5[c]	0.073	0.092	0.12	0.15
equilibrium binding[d]		0.043	0.025	1.4	0.58
RLL-EcMAT	0.0013	0.045	0.23	0.23	1.2
G8-EcMAT	0.0024	0.045	0.62	0.23	3.1
G7-EcMAT	0.0043	0.069	0.49	0.41	2.9
G6-EcMAT	0.0016	0.026	0.30	0.26	3.0
G5-EcMAT	0.0078	0.087	0.77	0.24	2.2
Rl-MAT[e]	0.03	0.25	0.13		
Rl-MAT[f]	0.58	∼1	0.12		

[a] MAT activity was measured as described under Experimental Procedures. Assays were performed at 22 °C in the presence in 50 mM Hepes•$(CH_3)_4N^+$ at pH 8.0 with 50 mM KCl, 50 mM $MgCl_2$. K_m is the concentration of substrate required for half-maximal activity at a saturating concentration of the second substrate, and K is the effective K_m extrapolated to zero concentration of the second substrate. The wild-type enzyme concentration was 0.3 μM, and the mutant enzyme concentrations were 10 μM. [b] Uncertainties in k_{cat} (moles of product formed per mole of enzyme active site per second) are within 15%, and uncertainties in K and K_m are within 30%. [c] 3 s^{-1} at 37 °C. [d] Data from McQueney et al. (*37*). [e] Tetramer, activity reported at 37 °C (*57*). [f] Dimer, activity reported at 37 °C (*56*). Complex kinetics with a lag phase in AdoMet formation were reported.

Kinetic Consequences of the Mutations. The kinetic constants for the overall AdoMet synthesis reaction, and for the tripolyphosphate hydrolytic reaction, are listed for all the enzymes studied in Tables 2 and 3, respectively. Since the AdoMet-forming step is both the rate-limiting step for k_{cat} in the overall reaction and is irreversible, only the PPP_i hydrolysis data report on late events in the reaction sequence. The results are illustrated in Figure 3. The kinetic data from simultaneous variation of ATP and methionine concentrations (25 concentration pairs) were analyzed to yield the K values for the substrates (effectively the K_m extrapolated to zero concentration of the second substrate) and the K_m at saturating concentration of the second substrate. The ratio of K/K_m reflects the synergistic effect of the binding of the first substrate on the affinity of the second substrate in this random kinetic mechanism. The ability of AdoMet to stimulate the rate of PPP_i hydrolysis was also determined as an additional probe of the effects of the mutations.

Effects of Swapping Natural Loop Sequences. The loop in Rl-MAT has a distinct sequence from that in EcMAT and is one residue longer. The variant in which the rat sequence HLDRNEEDV replaced the *E. coli* sequence is denoted RLL-EcMAT. RLL-EcMAT has a ∼1150-fold decrease in k_{cat} for AdoMet formation with <3-fold alteration in K_m values. The kinetic values reported for Rl-MAT have varied substantially, with recent data indicating a k_{cat} between ∼1% and ∼20% of the wild-type *E. coli* enzyme (*56*, *57*). Thus, part of the kinetic impairment arising from placing the rat loop sequence in the *E. coli* framework appears to reflect altered functioning in the context of the global *E. coli* protein environment. The ratio of K and K_m values reflects the synergistic effect of the cosubstrate on the saturation of the enzyme by the varied substrate. The ratio of 5 for K/K_m in RLL-EcMAT is 7-fold lower than the ratio of the corresponding constants for the wild-type enzyme, indicating a reduction of synergy in substrate binding. The increase in K for methionine and the decrease in K for ATP in the mutant suggest altered binding sites in the free enzyme, whereas

Table 3: Kinetic Parameters for Tripolyphosphatase Activity[a]

	−AdoMet			+AdoMet[b]			
enzyme	k_{cat} (s^{-1})	K_m (μM)	k_{cat}/K_m ($mM^{-1}\,s^{-1}$)	k_{cat} (s^{-1})	K_m (μM)	k_{cat}/K_m ($mM^{-1}\,s^{-1}$)	K_a(AdoMet)[c] (μM)
wild type	0.06	3	20	1.2	13	92	1.7
RLL-EcMAT	0.044	14	3.3	0.78	26	30	4.1
G8-EcMAT	0.079	1.6	49	1.2	8	150	4.1
G7-EcMAT	0.044	1.5	29	0.81	15	53	9.7
G6-EcMAT	0.022	3.2	6.9	0.84	11	76	3.8
G5-EcMAT	0.0023	5.3	0.43	0.52	24	22	4.3
Rl-MAT[d]	0.12	23	6.0				

[a] Tripolyphosphatase activity was measured in the presence and absence of AdoMet as described under Experimental Procedures. Uncertainties in k_{cat} values are within 15% and K_m or K_a values within 20%. The enzyme concentration was 2 μM in each case. [b] Measured in the presence of 100 μM AdoMet. [c] Concentration of AdoMet producing half-maximal change in the rate hydrolysis at 100 μM PPP_i. [d] Data from Lopez-Vara et al. (*56*) for the dimer at 37 °C. The PPP_i binding is cooperative with $n = 1.6$ in the absence of AdoMet, and 0.8 in the presence of AdoMet.

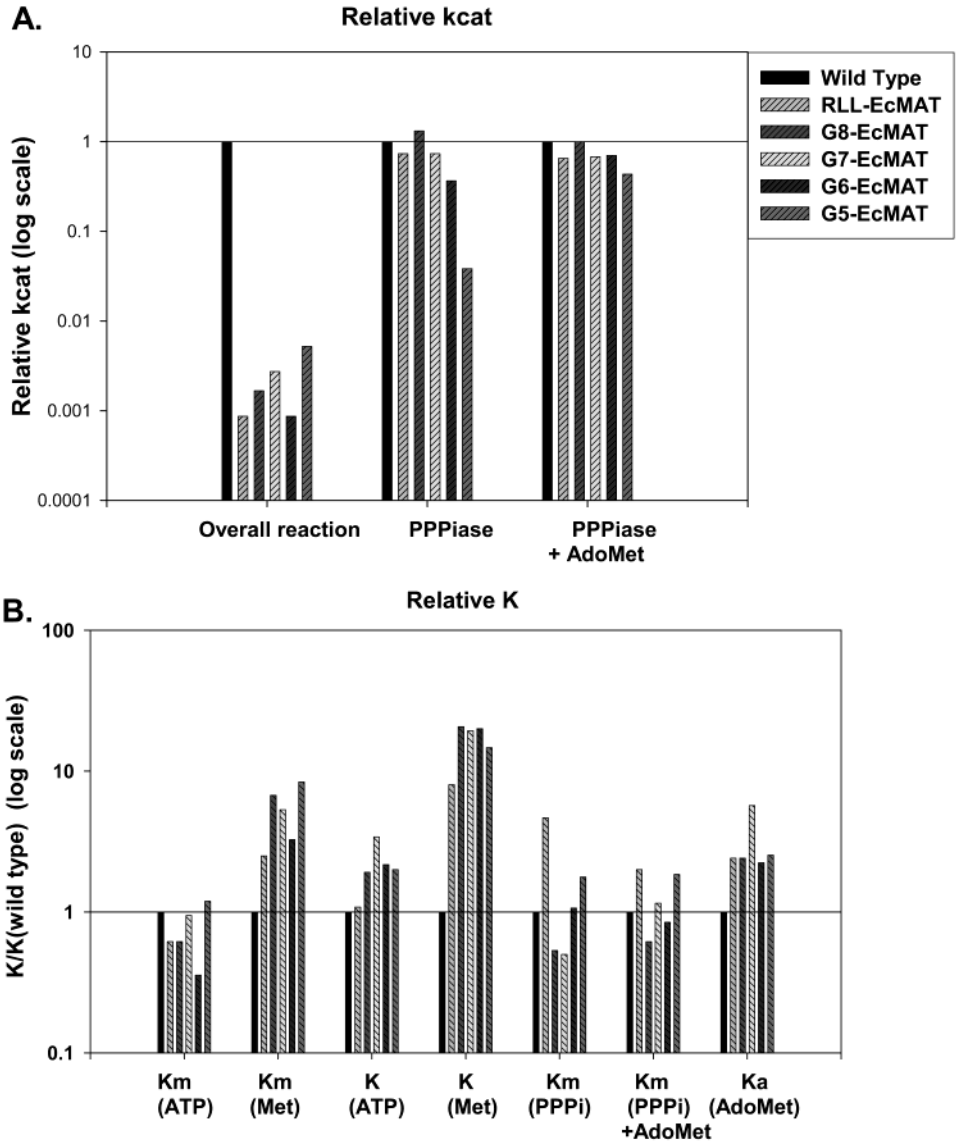

FIGURE 3: Effects of mutations on selected catalytic properties. (A) Comparison of the k_{cat} values for the overall MAT reaction and the PPP_i hydrolysis reaction in the absence and presence of AdoMet for the wild-type enzyme and the mutants described herein. (B) Relative K and K_m values for mutant and wild-type MATs are shown for ATP, methionine, PPP_i, PPP_i in the presence of AdoMet, and the concentration of AdoMet required for half-maximal stimulation of the PPP_i hydrolytic rate. Data from Tables 2 and 3 are presented on a logarithmic scale.

the K_m values indicate comparable saturation behaviors in formation of the ternary E·ATP·methionine complex.

In the tripolyphosphatase reaction, the RLL-EcMAT has a k_{cat} that is 1.5-fold reduced from wild-type EcMAT with a concomitant 5-fold increase in K_m; both kinetic parameters are similar to those reported for the native Rl-MAT [(*56*, *57*); Table 3]. When AdoMet is present as an activator of PPP_i hydrolysis, the kinetic values are similar to the wild-type EcMAT enzyme, with k_{cat} decreased by 1.5-fold and the K_m values increased by 2-fold; corresponding data for

the Rl-MAT are not available for comparison. Evidently the physical basis for AdoMet activation of the rate of PPP_i hydrolysis is retained in RLL-EcMAT. Thus, the properties of the RLL-EcMAT variant show that the loop functions largely in the AdoMet synthesis step of the reaction rather than in the subsequent reaction of PPP_i hydrolysis.

Loops Containing Oligoglycine. Oligoglycine-containing mutants were constructed and characterized in order to assess the importance of side chains in a loop of the same length as EcMAT, and the effects of loop length with the same sequence. The shortest length of five residues was chosen based on molecular modeling estimates of the minimum number of residues needed to connect the residues at the extremes of the disordered region in the E·ADP·P_i complex for which the α-carbons of D101 and R108 are separated by 16 Å [PDB file 1mxb (*32*)]. The oligoglycine mutants share several features that contrast with the wild-type EcMAT. In the overall reaction, k_{cat} values are reduced by 200−1000-fold. A 20−25-fold increase in the *K* value for methionine from the wild-type value was observed in all of the mutants, while there was a <2.5-fold increase in the corresponding *K* value for ATP (Table 2). The methionine K_m values for the G#-EcMAT are increased 3−8-fold from the EcMAT values, apparently as a result of the loss of the side chains in the loop. The K/K_m ratios reflect a 3−10-fold synergism in substrate binding; the extent of synergy does not parallel either the *K*, K_m, or k_{cat} values. The kinetic data for the oligoglycine mutants suggest comparable degrees of synergism in substrate binding among the mutants, but that synergism is decreased relative to the wild-type enzyme.

In the tripolyphosphatase reaction, for each mutant the k_{cat} and K_m values are less than 2-fold altered from the wild-type EcMAT when AdoMet is present, reinforcing the observation with the RLL-EcMAT that the loop constitution predominantly modulates the AdoMet-forming step in the overall reaction. In each case, the k_{cat} in the presence of AdoMet is greater than the k_{cat} for the overall reaction, demonstrating that an early step in the overall reaction is rate-limiting. The concentration of AdoMet required for half-maximal activation is increased by 2.5−5.7-fold, potentially reflecting the same phenomena as the increased *K* and K_m values for methionine. In the absence of AdoMet activation, the k_{cat} values for the oligoglycine mutants vary up to 30-fold, with less activity in mutants with shorter loops. There are less than 2-fold variations in K_m values. In the wild-type enzyme, the k_{cat} for PPP_i hydrolysis in the absence of AdoMet is limited by an early step in the reaction, apparently the chemical step itself (*37*). There is also a trend for the k_{cat} in the presence of AdoMet to decrease with loop shortening, although the magnitude of the effect is less; the intrinsic effect may be somewhat muted since the rate of product release is the same as the rate of the hydrolytic step in the presence of AdoMet, at least with the wild-type enzyme (*37*). The reductions in catalytic ability induced by the mutations are largely attenuated in the presence of AdoMet, as seen with the RLL-EcMAT variant, perhaps indicating that the decreased affinity for AdoMet reflects an increased use of binding energy in attaining the higher catalytic efficiency of the E·AdoMet·PPP_i complex.

Viscosity Dependence of the Kinetics of AdoMet Formation. The dependence of steady-state kinetic parameters on solution microvisosity has been used to investigate diffusional

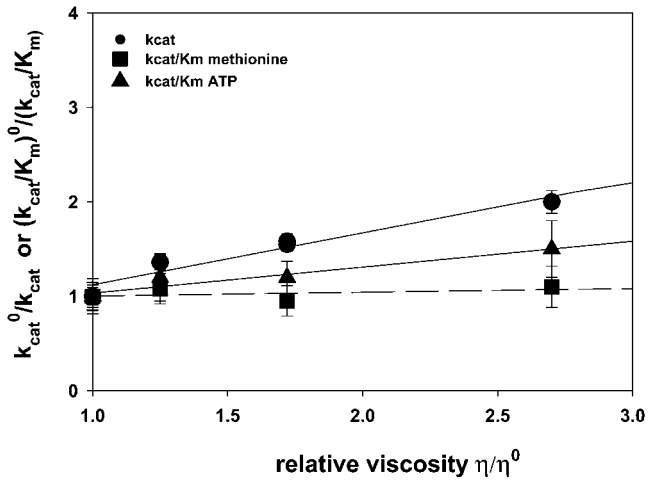

FIGURE 4: Viscosity dependence of k_{cat} and k_{cat}/K_m for the wild-type enzyme. The ratio of k_{cat} (or k_{cat}/K_m) determined at viscosity η to the corresponding value measured at the reference viscosity η^0 is plotted. Microviscosities were varied with sucrose at 0, 10, 20, and 30% (w/v). Lines are best fits to the data and indicate viscosity dependencies of 0.55, 0.27, and 0.05 for k_{cat}, k_{cat}/K_m(ATP) and k_{cat}/K_m(methionine), respectively. Other experimental conditions were as reported in Table 2.

contributions to enzymatic mechanisms (*7*, *21*, *22*, *24*, *29*, *58*−*61*). In addition to viscosity retardation of the diffusion of substrate/products to and from the active site, movements of protein segments may be slowed by enhanced viscosity, if the extent of reorganization is of sufficient magnitude (*24*). The viscosity dependence of the kinetics for the overall MAT reaction was examined using sucrose as microviscogen, and the results are illustrated in Figure 4. Control experiments with the macroviscogen Ficoll at a relative viscosity of 2.3 showed no alteration of k_{cat} or k_{cat}/K_m.

There is a clear dependence of k_{cat} on viscosity with the slope (k_{cat}^{η}) of 0.55 ± 0.06. In contrast, there is no significant effect of viscosity on k_{cat}/K_m for methionine, which is consistent with its dissociation rate ~10-fold greater than the catalytic rate; the measured value of $(k_{cat}/K_m)^{\eta}$ is 0.05 ± 0.15 for methionine (predicted value 0.09; see Experimental Procedures). For ATP, which has a dissociation rate only 3.5-fold faster than catalysis, $(k_{cat}/K_m)^{\eta}$ is 0.27 ± 0.05, in agreement with the predicted value of 0.25.

For the wild-type enzyme, both kinetic isotope effect studies and pre-steady-state kinetic measurements have shown that the chemical step of AdoMet formation is involved in the rate-limiting step of the reaction (*37*, *62*). The observation of a substantial dependence of k_{cat} on viscosity indicates that a diffusional event, such as loop movement, is tightly coupled to the chemical event, as was deduced for triosephosphate isomerase (*7*). Because the quantitative dependence of the rate of a conformational step on viscosity depends on the magnitude of the structural alteration, it is not possible to definitively deduce either the rate or the extent of the rearrangement directly from the value of k_{cat}^{η}. However, the knowledge that there is a conformational step coupled to AdoMet formation allows deductions about the kinetics of the step from other data (see Discussion). Unfortunately, in the presence of sucrose, the AdoMet determinations became unreliable at the 30-fold higher concentrations of mutant proteins required for kinetic measurements, preventing comparison of the viscosity dependencies of the mutant and wild-type enzymes.

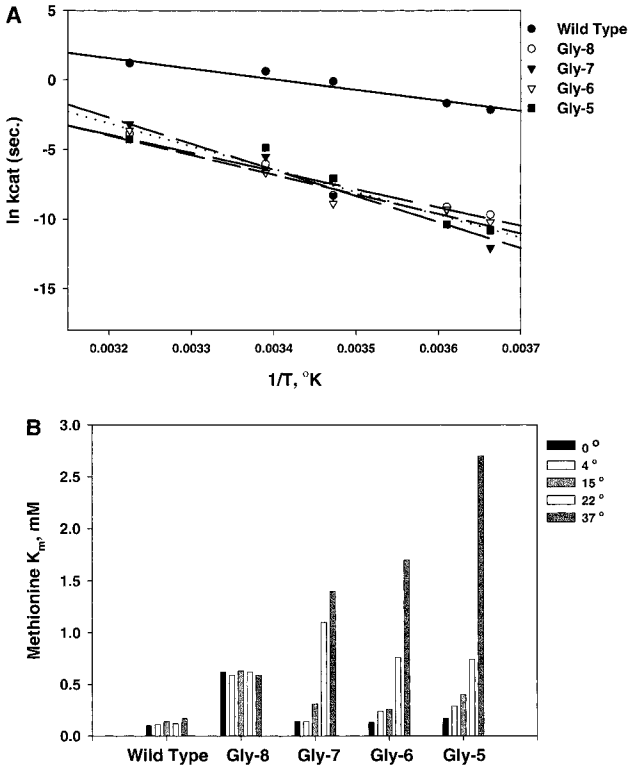

FIGURE 5: Temperature dependence of k_{cat} (part A) and the K_m for methionine (part B). Data are shown for the AdoMet synthesis reaction catalyzed by wild-type EcMAT and the G#-EcMAT mutants. The K_m for ATP increases ca. 3-fold with temperature in each case.

Mutational Effects on the Activation Energy of the MAT Reaction. The influence of the mutations on the thermodynamic parameters of catalysis was investigated by examination of the temperature dependence of the MAT reaction with the wild-type and oligoglycine mutants. Figure 5A shows Arrhenius plots for k_{cat}. The data were analyzed to yield the entropy, enthalpy, and free energy of activation ($\Delta S^{\#}_{310}$, $\Delta H^{\#}_{310}$, and $\Delta G^{\#}_{310}$, respectively) (Table 4). The activation energy is insignificantly different among the G#-EcMAT variants. The catalytic impairment of the mutants results from a ~2-fold increase in the enthalpy of activation, $\Delta H^{\#}_{310}$, from 14 to 25−36 kcal/mol, whereas the entropy of activation becomes favorable, $\Delta S^{\#}_{310}$ increasing from −10 cal/(mol·K) to a positive value in the range of +16 to +53 cal/(mol·K) (as a result of the propagation of errors in calculating $\Delta S^{\#}_{310}$, the values for the mutants are not significantly different from one another, but they are distinct from the value for the wild-type enzyme). The negative $\Delta S^{\#}_{310}$ in the wild-type enzyme-catalyzed reaction indicates an increase in the order of the system (enzyme + substrates + solvent) during the reaction transition state. In contrast, the positive value of $\Delta S^{\#}_{310}$ in the G#-EcMAT mutants indicates that the system becomes *less* ordered in the transition state. The loop in the glycine-8 mutant appears likely to have a wide range of energetically accessible conformations due to the absence of side chains, and a more positive $\Delta S^{\#}$ was unexpected given the anticipated ordering of the conformation during the reaction. One origin of the increase in entropy could be the release of bound waters from the active site if the protein assumes a closed conformation during catalysis. A dominant contribution from water release could be responsible for the comparable values of $\Delta S^{\#}$ for the mutants with varying length loops. Alternatively, in the mutants, the loop conformational distribution might not be altered during the reaction, thus removing the unfavorable entropic effects from loop rearrangements that occur during in the reaction catalyzed by the wild-type enzyme. The K_m for methionine was also found to increase with temperature, the change being larger in the G#-ECMAT variants with smaller numbers of glycines (Figure 5B). In contrast, the K_m for ATP increased 3-fold between 4 and 37 °C for each enzyme.

Table 4: Thermodynamic Parameters for k_{cat} in the AdoMet Synthetase Reaction[a]

	E_a (kcal/mol)[b]	$\Delta G^{\#}_{310}$ (kcal/mol)[c]	$\Delta H^{\#}_{310}$ (kcal/mol)[b]	$\Delta S^{\#}_{310}$ [cal/(mol·K)][d]
wild type EcMAT	14 ± 2	17	14	−10
G8-EcMAT	26 ± 4	20	25	16
G7-EcMAT	37 ± 6	20	36	53
G6-EcMAT	28 ± 4	20	28	22
G5-EcMAT	32 ± 4	21	32	36

[a] k_{cat} values were determined in the temperature range 0−37 °C; care was taken to ensure that substrate concentrations were saturating and that initial rates were measured. The activation energy, E_a, was calculated from the slope of the Arrhenius plot ($-E_a/R$). $\Delta G^{\#}$ was calculated from $\Delta G^{\#} = RT\,[\ln(k_B T/h) - \ln(k_{cat})]$ where $R = 1.9872$ cal/(mol·K), k_B is the Boltzmann constant, and h is Planck's constant. $\Delta H^{\#}$ was calculated as ($E_a - RT$). $\Delta S^{\#}$ was obtained as $(\Delta H^{\#} - \Delta G^{\#})/T$. [b] Errors in E_a and $\Delta H^{\#}$ reflect the errors in the slope of the Arrhenius plots. [c] Errors in $\Delta G^{\#}$ reflect errors in k_{cat} values and are with ±15% (Table 2). [d] $\Delta S^{\#}$ values contain uncertainties of 15 e.u. (wild type) to 25 e.u. (mutants) due to propagation of errors and are larger for the mutants as a result of the slower rates.

Modeling the Loop Mutational Effects. Since portions of the active site loop either are undefined in the available crystal structures or are locations that prevent substrate access to the active site, models were constructed of potential configurations of the wild-type loop and the glycine mutants. A conformational search for low-energy conformations of the wild-type loop was begun with the crystallographic coordinates and the torsional angles in the loop region varied (residues 98−116 in both subunits A and B). These residues were chosen because they encompassed both loop regions and two additional residues on either side. The energy of the EcMAT dimer [the minimal functional state of the enzyme (*40*)] in the lowest energy loop conformer found was 350 kcal/mol (1% of the total energy) less than the starting conformations, in part due to formation of 8 additional hydrogen bonds among loop residues in loop A (yielding a total of 13) and 12 additional hydrogen bonds in loop B (15 total). The two loops became more compact in the lower energy conformations, with the solvent-accessible surface areas for loops A and B of 1163 and 1492 Å^2 (total 26 932 Å^2 for the dimer (Figure 6A, red, black), compared to values of 1827 and 1621 Å^2 for the initial positions (Figure 6A, loop A in gray)). The main chain conformations of the loops in this model were more extended than in the original structure, as shown in Figure 6A. Another conformation of loop A, found starting from an arbitrary extended conformation of residues 102−107, had the same steric energy as that of the previously described loop A conformer but a much larger solvent-accessible surface area of 2123 Å^2 (Figure 6, green). The different conformations and comparable energies of the loops imply that the minimum energy conformation

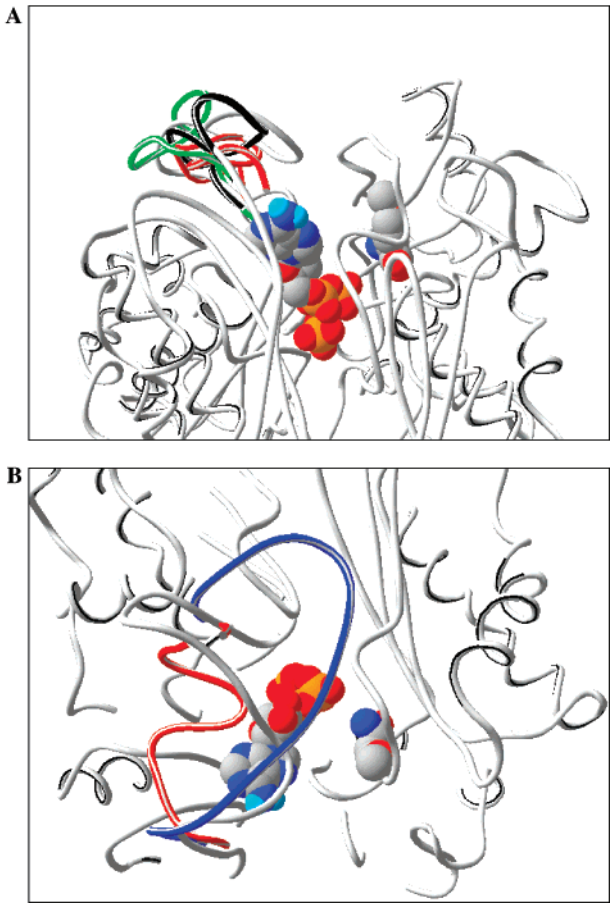

FIGURE 6: Models of alternate loop conformations. Part A: α-Carbon traces for the wild-type loop with crystallographically observed position (in gray) and the alternate conformations obtained from simulations (in green, red, and black; see text). Part B: The conformations modeled for the glycine-5 (in red) and glycine-8 mutants (in blue) are compared with those of the wild-type loop (gray). Cα traces are shown in each case, and the remainder of the protein is shown in gray. ADP, P_i, and cis-AMB are illustrated in space-filling models. The view in part B is from the top of the orientation in part A; a section through the protein is shown in part B to reduce background clutter.

may not be any of the conformations in these models. However, these models provide illustrations of potential topologies, and show that widely different conformations are energetically comparable. In the crystal structures with the loop disordered, the distance between the α-carbons of D101 and R108 is 16 Å, suggesting an extended conformation of the disordered region, whereas the separation is 12 Å in the crystal structure of the ligand-free enzyme; the distances are 10 and 14 Å in the two models of loop A and 17 Å in the model of loop B, indicating the backbone flexibility in this segment.

Models of potential conformers of the glycine-8 and glycine-5 mutants were also constructed based on the initial conformation of loop A in the apoenzyme, and are illustrated in Figure 6B (which is oriented so that the view is from the top of the orientation in Figure 6A). Deletion of the side chains reduces the solvent-accessible surface area of residues 98−116 by 400 Å^2 in the initial energy-minimized model of the G8-EcMAT; the solvent-accessible surface area for residues 98−113 in the glycine-5 model is smaller by an additional 100 Å^2. Since no hydrogen bonds were present among the side chains of loop A in the crystal structure (two hydrogen bonds are present in loop B, viz., Oδ of D107 to its own NH, and the main chain NH of Q104 to Oδ of N103), significant conformational alterations were not necessarily expected in the G8-EcMAT simulation. However, during the simulation of G8-EcMAT, the loop rearranged into a much more open form with loss of all five main chain hydrogen bonds (Figure 6B, blue). The solvent-accessible surface area decreased by only 40 Å^2, and the steric energy decreased by 50 kcal/mol compared to the energy of the initial energy-minimized conformation of the G8-EcMAT. The distance between the Cα of D101 and R108 increased substantially to 21 Å. In contrast, during the G5-EcMAT simulation, two additional main chain hydrogen bonds formed, and the solvent-accessible surface area decreased by 330 Å^2; the distance between the Cα of D101 and R108 remained 12 Å, indicative of the overall rigidity of this smaller loop.

DISCUSSION

The function of the mobile active site loop of MAT in catalytic function is clarified by the studies described herein. The combined results of the viscosity dependence of kinetic parameters and mutations are consistent with a kinetically significant conformational change that involves the active site loop during the AdoMet synthetic step. The global conformations of the loop mutant enzymes appear to be unchanged from the wild-type enzyme, as judged from the circular dichroism spectra, and the proteins remained tetramers; thus, the mutations had little effect on the overall protein structure, as anticipated from the surface location of the altered region. The replacement of the native *E. coli* loop sequence with the rat liver MAT sequence has a profound effect on the k_{cat} for the overall reaction, with little effect on the AdoMet-stimulated tripolyphosphatase rate or the K_m values. This demonstrates that the loop constitution is selectively important in catalysis of the first step in the overall reaction, AdoMet formation. The viscosity dependence of k_{cat} for the wild-type enzyme, which is determined by the rate of the E·ATP·methionine → E·AdoMet·PPP_i step, shows that this step is coupled to a viscosity-dependent conformational change. Since steps after AdoMet formation are not greatly altered by the mutations, the rate constants for the chemical step of k_5 and/or the associated conformational step k_{5iso} (see Figure 2 and below) have been altered in the mutants.

The properties of the oligoglycine mutants show that the length of the loop is in itself not a dramatic factor in determining the maximal catalytic activity, with differences in the AdoMet synthesis kinetics of less than 6-fold in k_{cat} and 3-fold in substrate synergism as the loop segment varies from five to eight residues. Even the most radical alteration, that of the GGGGG in G5-EcMAT, which we estimated would be the minimum peptide that could span the active site mouth in an open conformation, did not completely inactivate the enzyme by locking the active site closed (or open). In both triosephosphate isomerase and ribulose bisphosphate carboxylase/oxygenase, reducing the length of the active site loop by four to five residues resulted in $>10^5$-fold decreases in k_{cat}, and formation of aberrant reaction products, suggesting that in those enzymes loop closure is important in catalytic efficiency (*3, 10*). In contrast, the tripolyphosphatase activity of EcMAT is largely unaltered in the loop mutants and remains substantially faster than the

overall reaction; therefore, PPP_i formed as an intermediate is unlikely to escape from the active site.

The viscosity dependence of the kinetic parameters of the wild-type enzyme sheds another light on the dynamics of catalysis. The data show a dependence of k_{cat} on viscosity, with $k_{cat}^{\eta} = 0.55$. Thus, a viscosity-sensitive step, apparently a conformational change, occurs during the catalytic cycle after both substrates bind. Previous studies noted that the measured rate for methionine binding to the E·ATP complex is ~8-fold larger than that predicted from the k_{cat}/K_m, suggesting a unimolecular step after binding (*37*). However, in the absence of additional data, this step was not explicitly included in the mechanism (*37*). The current results provide independent support for a conformational change coupled to AdoMet formation, the step involving k_5 in Figure 2. Rate constants for this conformational change can be estimated from our published data. In the presence of isomerization of the ternary E·ATP·methionine complex, which either precedes or coincides with the irreversible chemical step of AdoMet formation (with rate constants $k_{\pm 5,iso}$), the net rate constant that determines the k_{cat}/K_m value for the path in which methionine binds to E·ATP is $k_{3'}$:

$$k_{3'} = k_3 k_{5,iso} k_5 / [k_{-3}(k_{-5,iso} + k_5) + k_{5,iso} k_5]$$

The forward rate constant, $k_{5,iso}$, must be as large as k_{cat}, and is probably greater, as reflected in the fully expressed ^{14}C kinetic isotope effect. The reverse rate constant, $k_{-5,iso}$, must be larger than k_{cat}, as revealed by the small amount of methionine isotope trapping. Estimating a lower limit for $k_{-5,iso}$ from the methionine dissociation rate constant of k_{-3}, 14 s^{-1}, and using $k_3 = 8k_{3'}$ (the difference in the observed binding rate constant and that calculated from the k_{cat}/K_m), then $k_{+5,iso}$ is calculated to be 22 s^{-1}, which is consistent with all the previous data in various publications. These lower limit values are remarkably similar to the rate constants for the isomerization associated with PPP_i binding to the E·SAM complex [forward rate constant $k_{-12,iso} = 33$ s^{-1}, reverse rate constant $k_{+12,iso} = 4$ s^{-1}(*37*)]. Thus, a conformational change coupled with AdoMet formation with forward and reverse rate constants both ca. 10-fold larger than k_{cat} is consistent with all of the available data. On the other hand, with estimates using the k_{cat} of 1.5 s^{-1} as a lower limit for $k_{+5,iso}$, then $k_{-5,iso}$ is calculated to be 0.95 s^{-1}, which is inconsistent with previous isotope trapping results that require a dissociation rate from the reactive form of the ternary complex of at least 10 s^{-1} (*37*). The viscosity dependence for k_{cat}/K_m of ATP is of the magnitude expected from the rate of dissociation of ATP. The viscosity independence of k_{cat}/K_m for methionine is also consistent with the previously measured dissociation rate.

Changes in substrate affinity due to binding site alterations were not anticipated since previous docking studies showed that the NMR-determined conformations of bound AdoMet and AMPPNP can bind in the same positions in the loop-open and loop-closed enzyme without contacting any loop residues (*63*). The methionine analogue inhibitor in the crystal structure of the rat liver enzyme would not be in direct contact with the loop residues if they are positioned similarly to the conformations in the ligand-free EcMAT structure. The loop models showed numerous conformations that are comparable in energy. However, none of these conformers place residues in positions to directly interact with the methionine binding site; rather, they remain closer to the ATP site. Thus, the observed increases in K and K_m values for methionine, but not those for ATP, were unexpected. The selective increases in the K values for methionine, and the associated decrease in k_{cat}/K_m, might be due either to a decreased binding rate or to an increased dissociation rate. The temperature dependence of the k_{cat}/K_m for methionine (but not the k_{cat}/K_m for ATP) differs with loop length, and is smaller in mutants with shorter loops because the increase in k_{cat} with temperature is offset by the increase in K_m. The magnitude of $\Delta S^{\#}$ for k_{cat}/K_m becomes smaller (less positive) as the loop length decreases, and all are more positive than the wild-type enzyme. The variations in $\Delta S^{\#}$ for k_{cat}/K_m with loop length are consistent with a decrease in the amount of water released in an early stage of the reaction, perhaps in conjunction with methionine binding, as the loop becomes shorter. Comparison of $\Delta S^{\#}$ for k_{cat} for the wild-type and mutant enzymes also reveals a more favorable entropy change in the reactions catalyzed by the mutants when the sequence is viewed from the E·ATP·methionine complex onward, but the variation among the mutant enzymes is not experimentally significant. The finding that $\Delta S^{\#}$ for k_{cat} is positive in the mutants and negative in the wild-type enzyme is consistent with a significant entropic contribution from solvent release in the mutant-catalyzed reactions, but a dominant effect from protein ordering in the wild-type system.

The substrate binding rates for the wild-type EcMAT are comparable for the free enzyme and the complexes in which the second substrate is already bound, suggesting that a gating action is not modulated on a time scale comparable to k_{cat} by the binding of the first substrate (*37*). However, a gating action of the loop, such that substrate association and dissociation only occur when the loop is open, could contribute to the relatively low substrate binding rates, and the retention of the PPP_i intermediate within the active site. In this case, the observed binding rate would be related to the binding rate for the loop-open form that exclusively has an accessible substrate site and the equilibrium between the open (E) and closed forms (E′, i.e., substrate-inaccessible form) by

$$E' \leftrightarrows E + S \leftrightarrows E{\cdot}S \rightarrow \rightarrow \rightarrow$$

where

$$E' = \text{closed and } E = \text{open}$$

and $k_{off-from-open} = (k_{on}/K_d)[(k_{open} + k_{closed})/k_{open}]$ where $k_{off} = k_{on}/K_d$ is the measured dissociation rate and $k_{off-from-open}$ is how fast dissociation occurs when the loop is open (*21*). The interconversion of E and E′ would have to occur with rates of at least 100 s^{-1} to have eluded our various studies to date.

The data for the wild-type enzyme suggest that upon formation of the E·AdoMet·PPP_i complex, either by chemical synthesis or by PPP_i binding (steps k_{+5} or k_{-12} in Figure 2), the loop is enticed to move, thus preventing rapid release of PPP_i or products from the active site. The similar values for the rate constants $k_{\pm 5,iso}$ and $k_{\pm 12,iso}$ suggest that these isomerizations are prompted by a common source, the electrostatic bait of the sulfonium cation which lures the loop

into the active site. This could be due to favoring a closed form of the loop that is already present in a preexisting conformational equilibrium, or formation of a conformation not present in the absence of AdoMet. Since the k_{cat} for PPP_i-ase in the presence of AdoMet is not altered in the mutants, and this k_{cat} is partly determined by product release for the wild-type enzyme, the rate for the conformational change $\mathcal{E}$·AdoMet·PP_i·P_i → E·AdoMet·PP_i·P_i that precedes product release, $k_{\pm 6,iso}$, cannot be greatly diminished in the mutants. However, this isomerization could be bypassed in the mutants if the previous conformational change leading to the E·AdoMet·PPP_i state does not occur in the early stage of the reaction. The altered loop in the mutants results in a less optimally organized active site, with reduced ability to catalyze AdoMet formation; this could result from the influence (or lack thereof) of the loop residues on the conformation of active site residues. The PPP_i hydrolysis reaction occurs in the protein interior, distant from the loop, and would be less disrupted by the mutations.

The properties of these mutants echo our previous observations with mutations of residues within the active site; i.e., mutations diminish the catalytic capability of the AdoMet-forming reaction to a larger degree than the PPP_i hydrolytic reaction (*38*, *64*, *65*). This property may reflect that many different active site structures are known that facilitate hydrolysis of polyphosphates, whereas the active site that catalyzes AdoMet formation appears to be highly specialized.

ACKNOWLEDGMENT

We thank Dr. Eileen K. Jaffe for helpful discussions.

REFERENCES

1. Joseph, D., Petsko, G. A., and Karplus, M. (1990) *Science 249*, 1425−1428.
2. Lolis, E., Alber, T., Davenport, R. C., Rose, D., Hartman, F. C., and Petsko, G. A. (1990) *Biochemistry 29*, 6609−6618.
3. Pompliano, D. L., Peyman, A., and Knowles, J. R. (1990) *Biochemistry 29*, 3186−3194.
4. Farnum, M. F., Magde, D., Howell, E. E., Hirai, J. T., Warren, M. S., Grimsley, J. K., and Kraut, J. (1991) *Biochemistry 30*, 11567−11579.
5. Li, L., Falzone, C. J., Wright, P. E., and Benkovic, S. J. (1992) *Biochemistry 31*, 7826−7833.
6. Sampson, N. S., and Knowles, J. R. (1992) *Biochemistry 31*, 8488−8494.
7. Sampson, N. S., and Knowles, J. R. (1992) *Biochemistry 31*, 8482−8487.
8. Kempner, E. S. (1993) *FEBS Lett. 326*, 4−10.
9. Gerstein, M., Lesk, A. M., and Chothia, C. (1994) *Biochemistry 33*, 6739−6749.
10. Larson, E. M., Larimer, F. W., and Hartman, F. C. (1995) *Biochemistry 34*, 4531−4537.
11. Williams, J. C., and McDermott, A. E. (1995) *Biochemistry 34*, 8309−8319.
12. Bell, C. E., and Eisenberg, D. (1996) *Biochemistry 35*, 1137−1149.
13. Muller, C. W., Schlauderer, G. J., Reinstein, J., and Schulz, G. E. (1996) *Structure 4*, 147−156.
14. Blake, C. (1997) *Nature 385*, 204−205.
15. Juszczak, L. J., Zhang, Z. Y., Wu, L., Gottfried, D. S., and Eads, D. D. (1997) *Biochemistry 36*, 2227−2236.
16. Landry, S. J., Steede, N. K., and Maskos, K. (1997) *Biochemistry 36*, 10975−10986.
17. Qian, M., Spinelli, S., Driguez, H., and Payan, F. (1997) *Protein Sci. 6*, 2285−2296.
18. Derreumaux, P., and Schlick, T. (1998) *Biophys. J. 74*, 72−81.
19. Veltman, O. R., Eijsink, V. G., Vriend, G., de Kreij, A., Venema, G., and Van den Burg, B. (1998) *Biochemistry 37*, 5305−5311.
20. Sun, J., and Sampson, N. S. (1999) *Biochemistry 38*, 11474−11481.
21. Wang, G. P., Cahill, S. M., Liu, X., Girvin, M. E., and Grubmeyer, C. (1999) *Biochemistry 38*, 284−295.
22. Huang, X., and Raushel, F. M. (2000) *Arch. Biochem. Biophys. 380*, 174−180.
23. Nelson, S. W., Choe, J. Y., Honzatko, R. B., and Fromm, H. J. (2000) *J. Biol. Chem. 275*, 29986−29992.
24. Kurz, L. C., Weitkamp, E., and Frieden, C. (1987) *Biochemistry 26*, 3027−3032.
25. Falzone, C. J., Wright, P. E., and Benkovic, S. J. (1994) *Biochemistry 33*, 439−442.
26. Zhou, H. X., Wlodek, S. T., and McCammon, J. A. (1998) *Proc. Natl. Acad. Sci. U.S.A. 95*, 9280−9283.
27. Bruice, T. C., and Benkovic, S. J. (2000) *Biochemistry 39*, 6267−6274.
28. Osborne, M. J., Schnell, J., Benkovic, S. J., Dyson, H. J., and Wright, P. E. (2001) *Biochemistry 40*, 9846−9859.
29. Shaffer, J., Sun, G., and Adams, J. A. (2001) *Biochemistry 40*, 11149−11155.
30. Fu, Z., Hu, Y., Markham, G. D., and Takusagawa, F. (1996) *J. Biomol. Struct. Dyn. 13*, 727−739.
31. Takusagawa, F., Kamitori, S., Misaki, S., and Markham, G. D. (1996) *J. Biol. Chem. 271*, 136−147.
32. Takusagawa, F., Kamitori, S., and Markham, G. D. (1996) *Biochemistry 35*, 2586−2596.
33. Mudd, S. H. (1973) in *The Enzymes*, 3rd ed., pp 21−154, Academic Press, New York.
34. Tabor, C. W., and Tabor, H. (1984) *Adv. Enzymol. 56*, 251−282.
35. Markham, G. D., Hafner, E. W., Tabor, C. W., and Tabor, H. (1980) *J. Biol. Chem. 255*, 9082−9092.
36. Gonzalez, B., Pajares, M. A., Hermoso, J. A., Alvarez, L., Garrido, F., Sufrin, J. R., and Sanz-Aparicio, J. (2000) *J. Mol. Biol. 300*, 363−375.
37. McQueney, M. S., Anderson, K. S., and Markham, G. D. (2000) *Biochemistry 39*, 4443−4454.
38. Reczkowski, R. S., Taylor, J. C., and Markham, G. D. (1998) *Biochemistry 37*, 13499−13506.
39. Kunkel, T. A. (1985) *Proc. Natl. Acad. Sci. U.S.A. 82*, 488−492.
40. Reczkowski, R. S., and Markham, G. D. (1995) *J. Biol. Chem. 270*, 18484−18490.
41. Taylor, J. C., Takusagawa, F., and Markham, G. D. (1996) *FASEB J. 10*, A970.
42. Baykov, A. A., Evtushenko, O. A., and Avaeva, S. M. (1988) *Anal. Biochem. 171*, 266−270.
43. Segel, I. H. (1975) in *Enzyme Kinetics. Behavior and Analysis of Rapid Equilibrium and Steady-State Enzyme Systems*, Wiley-Interscience, New York.
44. Cleland, W. W. (1979) *Methods Enzymol. 63*, 103−138.
45. Konkol, L., Hirai, T. J., and Adams, J. A. (2000) *Biochemistry 39*, 255−262.
46. McQueney, M. S., and Markham, G. D. (1995) *J. Biol. Chem. 270*, 18277−18284.
47. Weiner, S. J., Kollman, P. A., and Case, D. A. (1986) *J. Comput. Chem. 7*, 230−252.
48. Mohamadi, F., Richards, N. G. J., Guida, W. C., Liskamp, R., Lipton, M., Caufield, C., Chang, G., Hendrickson, T., and Still, W. C. (1990) *J. Comput. Chem. 11*, 440−467.
49. McDonald, D. Q., and Still, W. C. (1992) *Tetrahedron Lett. 33*, 7743−7746.
50. Qiu, D., Shenkin, P. S., Hollinger, F. P., and Still, W. C. (1997) *J. Phys. Chem. A 101*, 3005−3014.
51. Kolossvary, I., and Guida, W. C. (1996) *J. Am. Chem. Soc. 118*, 5011−5019.
52. Kolossvary, I., and Keseru, G. M. (2001) *J. Comput. Chem. 22*, 21−30.
53. Branchini, B. R., Magyar, R. A., Murtiashaw, M. H., and Portier, N. C. (2001) *Biochemistry 40*, 2410−2418.
54. Branchini, B. R., Magyar, R. A., Murtiashaw, M. H., Anderson, S. M., and Zimmer, M. (1998) *Biochemistry 37*, 15311−15319.
55. Branchini, B. R., Magyar, R. A., Murtiashaw, M. H., Anderson, S. M., Helgerson, L. C., and Zimmer, M. (1999) *Biochemistry 38*, 13223−13230.
56. Lopez-Vara, M. C., Gasset, M., and Pajares, M. A. (2000) *Protein Expression Purif. 19*, 219−226.
57. Sanchez Del Pino, M. M., Corrales, F. J., and Mato, J. M. (2000) *J. Biol. Chem. 275*, 23476−23482.
58. Hardy, L. W., and Kirsch, J. F. (1984) *Biochemistry 23*, 1275−1282.

59. Hirai, T. J., Tsigelny, I., and Adams, J. A. (2000) *Biochemistry 39*, 13276−13284.
60. Blacklow, S. C., Raines, R. T., Lim, W. A., Zamore, P. D., and Knowles, J. R. (1988) *Biochemistry 27*, 1158−1167.
61. Adams, J. A., and Taylor, S. S. (1992) *Biochemistry 31*, 8516−8522.
62. Markham, G. D., Parkin, D. W., Mentch, F., and Schramm, V. L. (1987) *J. Biol. Chem. 262*, 5609−5615.
63. Schalk-Hihi, C., and Markham, G. D. (1999) *Biochemistry 38*, 2542−2550.
64. Taylor, J. C., and Markham, G. D. (1999) *J. Biol. Chem. 274*, 32909−32914.
65. Taylor, J. C., and Markham, G. D. (2000) *J. Biol. Chem. 275*, 4060−4065.

BI025851T